Some reversing orbits for a rattleback model

Gianni Arioli [1,2] and Hans Koch [3]

Abstract. A physical rattleback is a toy that can exhibit counter-intuitive behavior when spun on a horizontal plate. Most notably, it can spontaneously reverse its direction of rotation. Using a standard mathematical model of the rattleback, we prove the existence of reversing motion, reversing motion combined with rolling, and orbits that exhibit such behavior repeatedly.

1. Introduction

We consider the frictionless motion of a solid three-dimensional ellipsoid that is in no-slip contact with a fixed horizontal plate and subject to a vertical gravitational force. If the solid is homogeneous, then the axes of inertia agree with the geometric axes of the ellipsoid. In this case, the equations of motion can be solved explicitly [3]. More interesting behavior is observed when the axes of inertia are rotated by a nonzero angle δ about the geometric axis that corresponds to smallest diameter of the ellipsoid [1]. This is a standard model for the so-called rattleback or Celtic stone, where δ is usually chosen close to zero [2,8]. Like the homogeneous ellipsoid, it admits a rotating motion with constant angular velocity about the vertical axis, if this axis corresponds to smallest diameter of the body. But if this angular velocity (lies withing a certain range and) gets perturbed in a non-vertical direction, then the rotation is observed to gradually slow down and eventually reverse direction. The reversal is accompanied by a rattling motion, whence the name rattleback. Some videos of such reversing orbits are posted at [22].

This behavior is somewhat counter-intuitive and appears to violate conservation of angular momentum. But angular momentum can be exchanged with the plate; and if the center of gravity is not vertically above the contact point, then the resulting torque can slow down rotation and even reverse its direction. (There is a preferred direction that is related to the sign of δ.) For a more detailed description of the rattleback reversal, the underlying physics, numerical experiments, and more, we refer to [6,9,13,14,15,17,18] and references therein.

Similar behavior is observed, both in physical models and numerical experiments, for rattlebacks whose bodies are cut-off elliptic paraboloids. But to our knowledge, there are no rigorous results in either case that establish the existence of reversing orbits. In this paper, we prove the existence of such orbits, including orbits that are periodic and thus reverse infinitely often. Our presentation is self-contained and can serve as an introduction to the rattleback model for a mathematically oriented reader.

To be more specific, let us first introduce the equation of motion. The position of a rigid body in $\mathbb{R}^3$ can be described by specifying its center of mass G and an orthonormal 3×3 matrix Q representing a rotation about G. The unit vector $\boldsymbol{e}_3 = [0\ 0\ 1]^\top$ will be referred to as the vertical direction. Here, and in what follows, $A^\top$ denotes the transpose

[1] Department of Mathematics, Politecnico di Milano, Piazza Leonardo da Vinci 32, 20133 Milano.

[2] Supported in part by the PRIN project "Equazioni alle derivate parziali e disuguaglianze analitico-geometriche associate".

[3] Department of Mathematics, The University of Texas at Austin, Austin, TX 78712.

of a matrix A. The corresponding vertical direction in the body-fixed frame is the third column $\boldsymbol{\gamma} = Q\boldsymbol{e}_3$ of the matrix Q. Consider now a body that is moving as a function of time t, and denote by $\frac{d}{dt}\boldsymbol{x}$ or $\dot{\boldsymbol{x}}$ the time-derivative of a vector-valued function $\boldsymbol{x}$. Then $\frac{d}{dt}Q^\top \boldsymbol{x} = Q^\top \boldsymbol{x}'$, where $\boldsymbol{x}' = \dot{\boldsymbol{x}} - \boldsymbol{x} \times \boldsymbol{\omega}$. Here, $\boldsymbol{\omega}$ is the angular velocity about G, and $\boldsymbol{a} \times \boldsymbol{b}$ denotes the cross product of two vectors $\boldsymbol{a}$ and $\boldsymbol{b}$ in $\mathbb{R}^3$.

In the case of the rattleback with mass m, a vertical gravitational force $-mg\boldsymbol{\gamma}$ acts at the center of mass G, where g is a gravitational acceleration. Suppose that the body stays in contact with a fixed horizontal plate and satisfies a no-slip condition $\boldsymbol{v} = \boldsymbol{r} \times \boldsymbol{\omega}$. Here, $\boldsymbol{v}$ is the velocity of G and $\boldsymbol{r}$ denotes the vector from G to the point of contact C. Assuming conservation of momentum, we have $m\boldsymbol{v}' = \boldsymbol{f} - mg\boldsymbol{\gamma}$, where $\boldsymbol{f}$ is the force exerted on the body at C. Assuming conservation of angular momentum as well, we have $(\mathbb{I}\,\boldsymbol{\omega})' = \boldsymbol{r} \times \boldsymbol{f}$, where $\mathbb{I}$ is the inertia tensor about G.

Notice that $\boldsymbol{r} \times \boldsymbol{f} = m\boldsymbol{r} \times \boldsymbol{v}' + mg\boldsymbol{r} \times \boldsymbol{\gamma}$ due to momentum conservation. Substituting this expression into the equation $(\mathbb{I}\,\boldsymbol{\omega})' = \boldsymbol{r} \times \boldsymbol{f}$, we end up with the equation of motion

$$\mathbb{I}\,\dot{\boldsymbol{\omega}} - (\mathbb{I}\,\boldsymbol{\omega}) \times \boldsymbol{\omega} = m\boldsymbol{r} \times \dot{\boldsymbol{v}} - m\boldsymbol{r} \times (\boldsymbol{v} \times \boldsymbol{\omega}) + mg\boldsymbol{r} \times \boldsymbol{\gamma}\,. \tag{1.1}$$

In addition, we have $\dot{\boldsymbol{\gamma}} = \boldsymbol{\gamma} \times \boldsymbol{\omega}$, due to the fact that $\boldsymbol{\gamma}' = \boldsymbol{0}$. The dynamic variables here are $\boldsymbol{\gamma}$ and $\boldsymbol{\omega}$. For the velocity $\boldsymbol{v}$ we can substitute $\boldsymbol{r} \times \boldsymbol{\omega}$, and the vector $\boldsymbol{r}$ can be expressed in terms of $\boldsymbol{\gamma}$ by using the geometry of the body.

In this paper, we consider the body to be an ellipsoid in $\mathbb{R}^3$ with principal semi-axes $b_1 > b_2 > b_3 > 0$. Consider the 3×3 matrix $B = \operatorname{diag}(b_1, b_2, b_3)$. Then the equation for the surface of the body and the tangency condition at the point of contact C are given by

$$F(\boldsymbol{r}) = 1\,, \qquad \nabla F(\boldsymbol{r}) = -\|\nabla F(\boldsymbol{r})\|\boldsymbol{\gamma}\,, \qquad F(\boldsymbol{r}) \stackrel{\text{def}}{=} \left\|B^{-1}\boldsymbol{r}\right\|^2. \tag{1.2}$$

Using these equations, one easily finds that

$$\boldsymbol{r} = -s^{-1}B^2\boldsymbol{\gamma}\,, \qquad s \stackrel{\text{def}}{=} \|B\boldsymbol{\gamma}\|\,. \tag{1.3}$$

The inertia tensor $\mathbb{I}$ is assumed to be a strictly positive symmetric 3×3 matrix. Then $\mathbb{I}$ is invertible, and (1.1) together with the equation $\dot{\boldsymbol{\gamma}} = \boldsymbol{\gamma} \times \boldsymbol{\omega}$ defines a flow on $\mathbb{R}^6$. This flow preserves the length $\ell = \|\boldsymbol{\gamma}\|$. A straightforward computation shows that another flow-invariant quantity is the total energy

$$\mathcal{H} = \tfrac{1}{2}\boldsymbol{\omega}^\top \mathbb{I}\,\boldsymbol{\omega} + \tfrac{1}{2}m\|\boldsymbol{v}\|^2 + mgs\,. \tag{1.4}$$

The three terms on the right hand side of this equation can be identified with the rotational kinetic energy, the translational kinetic energy, and the potential energy, respectively. We note that the no-slip condition $\boldsymbol{v} = \boldsymbol{r} \times \boldsymbol{\omega}$ is a non-holonomic constraint, so the rattleback model is not a Hamiltonian system.

In what follows, we restrict to $\|\boldsymbol{\gamma}\| = 1$, unless specified otherwise. Then the phase space for our flow is $\mathbb{S}_2 \times \mathbb{R}^3$, where $\mathbb{S}_2$ denotes the unit sphere in $\mathbb{R}^3$. The dimension can be reduced further from 5 to 4, if desired, by choosing an energy $E > mgb_3$ and restricting to the fixed-energy surface

$$\mathcal{M}_E = \left\{x \in \mathcal{M} : \mathcal{H}(x) = E\right\}, \qquad \mathcal{M} = \mathbb{S}_2 \times \mathbb{R}^3\,. \tag{1.5}$$

Clearly, these invariant surfaces are all compact. So in particular, every orbit returns arbitrarily close to a point that it has visited earlier. This allows for a variety of different types of motion, including periodic, quasiperiodic, and chaotic orbits. For the parameters and energies considered in this paper, orbits that look periodic are abundant. However, finding nontrivial periodic orbits turns out to difficult, unless one focuses on reversible orbits.

An important feature of the rattleback flow is reversibility. To be more precise, let Φ be the flow for some vector field X on $\mathbb{R}^n$. That is, $\frac{d}{dt}\Phi_t = X \circ \Phi_t$ for all $t \in \mathbb{R}$. Given an invertible map R on $\mathbb{R}^n$, we say that Φ is R-reversible if $R \circ \Phi_t = \Phi_{-t} \circ R$ for all times t. Reversible dynamical systems share many qualitative properties with Hamiltonian dynamical systems [4,5,10,12]. But they need not preserve a volume. In fact, one of our results exploits the existence of stationary solutions that attract (or repel) nearby points with the same energy. Nontrivial attractors of the type seen in dissipative systems have been observed numerically e.g. in [13,14,17].

A well-known consequence of R-reversibility is the following. Assume that Φ is R-reversible, and that some orbit of Φ includes two distinct points x and $\Phi_\tau(x)$ that are both R-invariant. Then the orbit is time-periodic with period 2τ. The proof is one line:

$$\Phi_{2\tau}(x) = \Phi_\tau(\Phi_\tau(x)) = \Phi_\tau(R(\Phi_\tau(x))) = \Phi_\tau(\Phi_{-\tau}(R(x))) = R(x) = x\,. \tag{1.6}$$

This property will be used to construct symmetric periodic orbits for the rattleback flow.

It is well-known that the rattleback flow is R-reversible for the reflection

$$R(\boldsymbol{\gamma}, \boldsymbol{\omega}) = (\boldsymbol{\gamma}, -\boldsymbol{\omega})\,. \tag{1.7}$$

Here, and in what follows, we use the notation $(x_1, \ldots, x_n) = [x_1 \ \ldots \ x_n]^\top$ for vectors in $\mathbb{R}^n$. A rattleback with ellipsoid geometry (1.2) has another symmetry: the flow commutes with the reflection $S_0(\boldsymbol{\gamma}, \boldsymbol{\omega}) = (-\boldsymbol{\gamma}, \boldsymbol{\omega})$. Additional symmetries exist for special choices of the inertia tensor $\mathbb{I}$. A standard choice in experiments is to take $\mathbb{I}_{13} = \mathbb{I}_{23} = 0$. Then the system is invariant under a rotation by π about the vertical axis $\boldsymbol{e}_3$. In what follows, we always restrict to this situation. As a consequence, the flow commutes with the reflection $S(\boldsymbol{\gamma}, \boldsymbol{\omega}) = ((-\gamma_1, -\gamma_2, \gamma_3), (-\omega_1, -\omega_2, \omega_3))$. And it commutes with the reflection $S' = SS_0$ as well. Given that S' commutes with R, our flows are RS'-reversible, where

$$RS'(\boldsymbol{\gamma}, \boldsymbol{\omega}) = \big((\gamma_1, \gamma_2, -\gamma_3), (\omega_1, \omega_2, -\omega_3)\big)\,. \tag{1.8}$$

As part of our investigation, we have carried out numerical simulations for various choices of the model parameters. For simplicity, we focus here on a single set of parameters, namely

$$\begin{array}{rclrclrclrcl} m &=& 4\,, & b_1 &=& 5\,, & b_2 &=& \frac{17}{16}\,, & b_3 &=& 1\,, \\ \mathbb{I}_{11} &=& \frac{2223}{1024}\,, & \mathbb{I}_{12} &=& -\frac{3021}{1024}\,, & \mathbb{I}_{22} &=& \frac{2603}{128}\,, & \mathbb{I}_{33} &=& \frac{669}{32}\,, \end{array} \tag{1.9}$$

and $\mathbb{I}_{13} = \mathbb{I}_{23} = 0$. For the gravitational acceleration we choose the value $g = \frac{40141}{4096}$. These parameters can be realized in a physical experiment, with the proper choice of units for length, mass, and time. (Possible units would be centimeters, decagrams, and deciseconds,

respectively.) We note that the matrix $\mathbb{I}$ is strictly positive, and that the smallest possible energy of a point in $\mathcal{M}$ is $mgb_3 = \frac{40141}{1024} = 39.2001953125$.

The chosen inertia tensor is of the form $\mathbb{I} = \mathcal{R}^{-1}\mathbb{I}_0\mathcal{R}$, where $\mathbb{I}_0$ is roughly the inertia tensor of a homogeneous solid ellipsoid with the given mass m and semi-axes b_j, and where $\mathcal{R}$ is a rotation about the vertical axis $\boldsymbol{e}_3$ by an angle $\delta \simeq \frac{\pi}{20}$.

2. Main results

A trivial solution of the rattleback equation is the stationary solution with $\boldsymbol{\gamma} = (0, 0, 1)$ and $\boldsymbol{\omega} = (0, 0, \omega_3)$. If $\omega_3 \neq 0$, then this corresponds to a steady rotation about the vertical axis. As mentioned earlier, one of the peculiar features of the rattleback is observed when starting with a nearby initial condition that is not a stationary point. If ω_3 is within a certain range of values, then the rotation is observed to slow down and eventually reverse direction. In order to give a precise definition of reversal, consider the column vectors $\boldsymbol{\alpha}$, $\boldsymbol{\beta}$, and $\boldsymbol{\gamma}$ of the rotation matrix Q, and define the angle ψ_0 by the equation

$$\tan\psi_0 = \frac{\alpha_1}{\beta_1}\,, \qquad \psi_0 \in \mathbb{R}/(\pi\mathbb{Z})\,. \tag{2.1}$$

When evaluated along an orbit, this "yaw-angle" ψ_0 typically varies as a function of time. Denote by $\psi : \mathbb{R} \to \mathbb{R}$ a continuous lift of ψ_0 to the real line. We say that the body reverses its direction of rotation on a time interval $[a, b]$, if there exists a time $c \in [a, b]$ such that the differences $\psi(c) - \psi(a)$ and $\psi(c) - \psi(b)$ have the same sign and are bounded away from zero by some positive constant C. The largest such constant C will be referred to as the amplitude of the reversal, and the sign of $\psi(c) - \psi(a)$ will be called the sign of the reversal.

Theorem 2.1. *There exists an R-symmetric periodic orbit of period $T = 227.471\ldots$ that reverses its direction of rotation on $[-T/2, T/2]$ and on $[0, T]$, with opposite signs and amplitudes larger than 4. The energy for this orbit is $E = 39.683\ldots$*

Our proof of this theorem is computer-assisted, in the sense that it involves estimates that have been verified (rigorously) with the aid of a computer. The same applies to the theorems stated below. The statement $E = 39.683\ldots$ in Theorem 2.1 means that $39.683 \leq E < 39.684$. The same notation is used for other interval enclosures. We note that our actual bounds are much more accurate.

The orbit mentioned in Theorem 2.1 is depicted in Figure 1. To be more precise, consider the angular velocity $\boldsymbol{M} = \mathbb{I}\,\boldsymbol{\omega} - m\boldsymbol{r} \times \boldsymbol{v}$ about the contact point C. This angular velocity has been used as primary variable (in place of $\boldsymbol{\omega}$) in several papers. A straightforward computation shows that

$$\boldsymbol{M} = [\mathbb{I} + mK(\boldsymbol{r})]\boldsymbol{\omega}\,, \qquad K(\boldsymbol{r}) = \|\boldsymbol{r}\|^2\mathrm{I} - \boldsymbol{r}\boldsymbol{r}^\top\,. \tag{2.2}$$

The matrix $\mathbb{I} + mK(\boldsymbol{r})$ is strictly positive, so (2.2) could be used to express $\boldsymbol{\omega}$ in terms of $\boldsymbol{M}$. We note that the reflections R, S, and S' commute with the change of variables $(\boldsymbol{\gamma}, \boldsymbol{\omega}) \mapsto (\boldsymbol{\gamma}, \boldsymbol{M})$.

Figure 1 shows the components of $\boldsymbol{\gamma}$ (left) and of $\boldsymbol{M}$ (right) as functions of time t, for the orbit described in Theorem 2.1. The R-reversibility of the orbit is equivalent to the condition that $\boldsymbol{\gamma}$ is an even function of t, while $\boldsymbol{M}$ is an odd function of t.

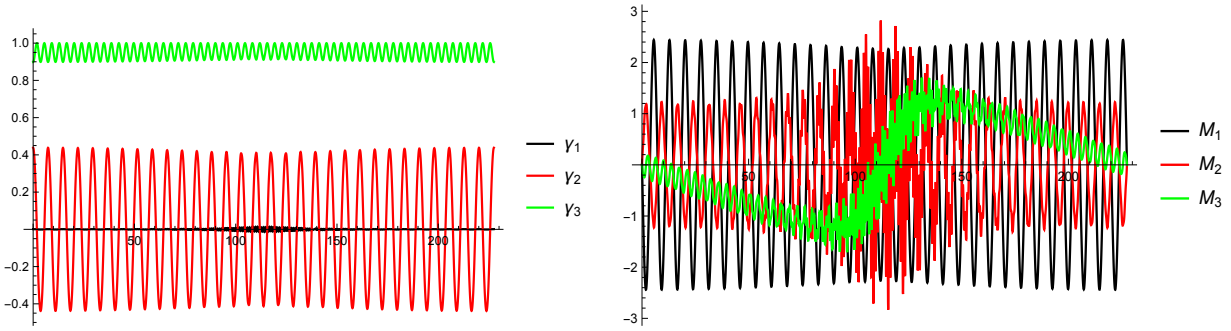

Figure 1. Components γ_j (left) and M_j (right) for the orbit described in Theorem 2.1.

Remark 1. All of our results that refer to the parameters (1.9) hold for an open set of parameter values nearby. This is a consequence of nondegeneracy properties that are verified as part of our proofs.

Our next result concerns the existence of a reversing heteroclinic orbit between two stationary points of the form $z_c = (\boldsymbol{e}_3, c\,\boldsymbol{e}_3)$. As will be shown in the next section, there exists a value $c_* = 1.048\ldots$ such that z_c is repelling for $c < -c_*$ and attracting for $c > c_*$, if the flow is restricted to the surface of fixed energy $E = \mathcal{H}(z_c)$.

Theorem 2.2. *Consider the parameter values (1.9). For $c = 1.849\ldots$ there exists a heteroclinic R-reversible orbit connecting z_{-c} to z_c. This orbit reverses its direction of rotation on $[-b, b]$ for large $b > 0$, and the amplitude tends to infinity as $b \to \infty$. An analogous orbit (in fact a one-parameter family) exists for $c = 1.467\ldots$ that is RS-reversible. The energies of these two orbits are $E = 74.95\ldots$ and $E = 61.72\ldots$, respectively.*

The first orbit described in this theorem is depicted in Figure 2. We note that this orbit must pass through an R-invariant point x at time $t = 0$. Since z_{-c} is repelling and z_c attracting (for fixed energy), every point that is sufficiently close to x and has the same energy as x lies on some heteroclinic orbit connecting z_{-c} to z_c. We expect that there exists heteroclinic orbits between $z_{\pm c}$ for a range of values $c > c_*$, and it is possible that such orbits exist for some range of values $c < c_*$ as well.

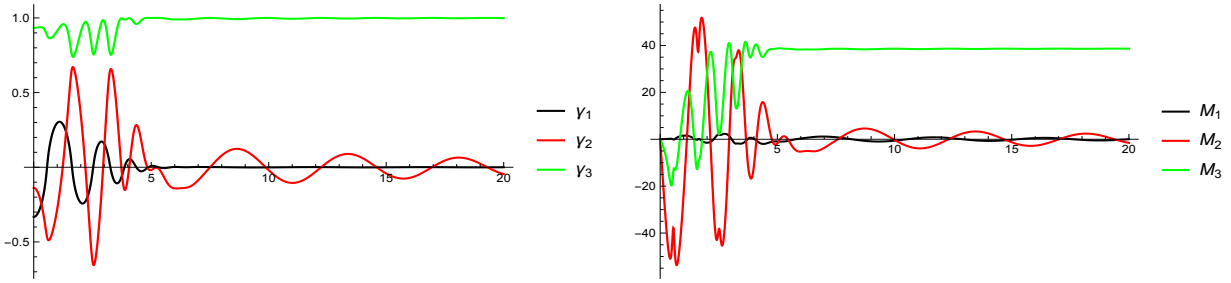

Figure 2. Components γ_j (left) and M_j (right) for the first orbit described in Theorem 2.2.

Numeral experiments are most often carried out for rattlebacks whose body is a cut-off elliptic paraboloid. If we replace $F(\boldsymbol{r}) = \|\boldsymbol{\rho}\|^2$ by $F(\boldsymbol{r}) = \rho_1^2+\rho_2^2-2\rho_3-1$, where $\boldsymbol{\rho} = B^{-1}\boldsymbol{r}$, then the behavior can be expected to be similar to the behavior of the ellipsoid, as long as $\boldsymbol{\gamma}$ stays close to $\boldsymbol{e}_3$. Among the features of the ellipsoid-shaped rattleback that cannot be studied in the cut-off paraboloid case is roll-over motion.

A possible definition of "rolling over $\boldsymbol{e}_1$" can be given in terms of the angle ϕ_0 defined by the equation

$$\tan\phi_0 = \frac{\gamma_2}{\gamma_3}\,, \qquad \phi_0 \in \mathbb{R}/(\pi\mathbb{Z})\,. \tag{2.3}$$

When evaluated along an orbit, this "roll-angle" ϕ_0 typically varies as a function of time. Denote by $\phi : \mathbb{R} \to \mathbb{R}$ a continuous lift of ϕ_0 to the real line. We say that the body rolls over $\boldsymbol{e}_1$ on a time interval $[a, b]$, if the difference $\phi(b) - \phi(a)$ is no less than π in absolute value. The sign of $\phi(b) - \phi(a)$ will be called the direction of the roll-over.

Theorem 2.3. *Consider the parameter values (1.9). There exists a periodic orbit of period $T = 254.286\ldots$ that rolls over $\boldsymbol{e}_1$ on two time-intervals, once in the positive direction, and once in the negative direction. In addition, the orbit reverses its direction of rotation on $[-T/2, T/2]$ and on $[0, T]$, with opposite signs and amplitudes larger than 24. The orbit is R-symmetric, and when translated in time by $T/4$, it becomes RS'-symmetric. Its energy is $E = 42.0308\ldots$ Furthermore, there exists a one-parameter family of such orbits.*

The orbit described in this theorem is depicted in Figures 3 and 4.

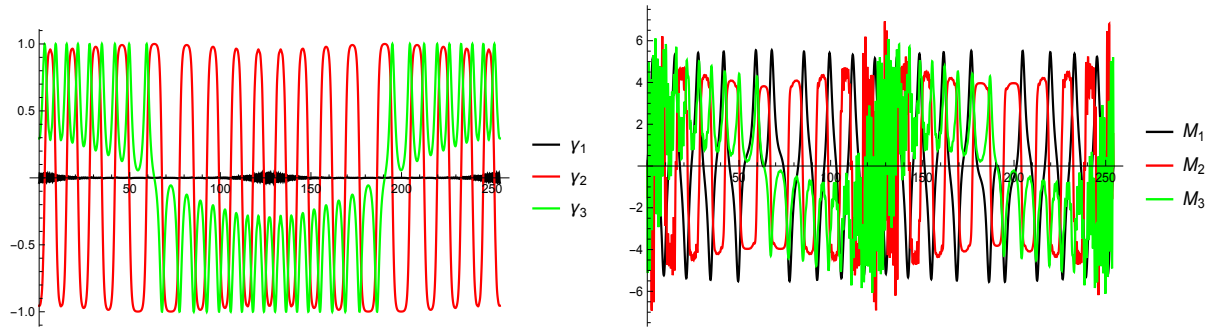

Figure 3. Components γ_j (left) and M_j (right) for the orbit described in Theorem 2.3.

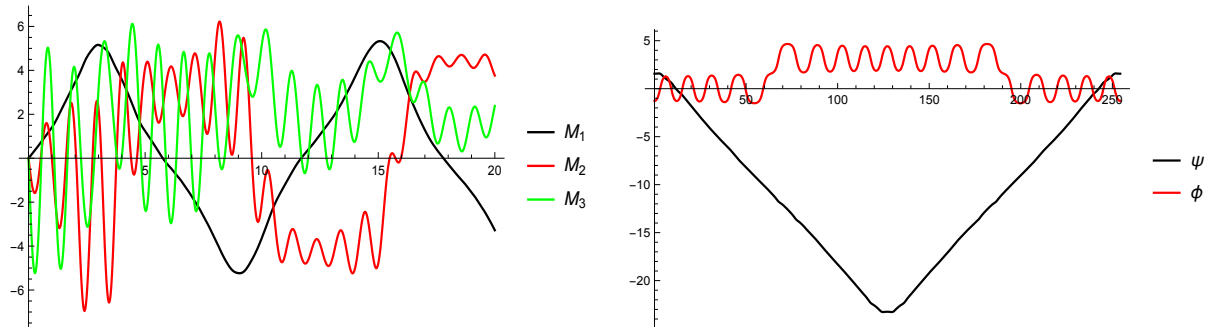

Figure 4. Components M_j (left) and angles ψ, ϕ (right) for the orbit described in Theorem 2.3.

The right part of Figure 4 shows the lifted yaw-angle ψ and the lifted roll-angle ϕ. The left part shows the behavior of $\boldsymbol{M}$ near $t = 0$. It illustrates e.g. that the rattleback motion exhibits many rapid variations, especially during reversals. Controlling such orbits rigorously involves rather accurate estimates. Typical error bounds in our analysis are of the order 2^{-2000}.

3. Some simpler solutions

After describing a periodic orbit that rolls over $\boldsymbol{e}_1$ repeatedly in the same direction, we will discuss some stationary solutions and their stability.

Theorem 3.1. *Consider the parameter values (1.9). There exists a RS'-symmetric periodic orbit of period $T = 18.061\ldots$ and energy $E = 42.99\ldots$ that rolls over $\boldsymbol{e}_1$ on two adjacent time-intervals of combined length T, both times with the same direction. In fact, there exists a two-parameter family of such orbits.*

The orbit described in this theorem is depicted in Figure 5. Our numerical results suggest that both the yaw-angle ψ and the roll-angle ϕ are monotone for this orbit, but we did not try to prove this.

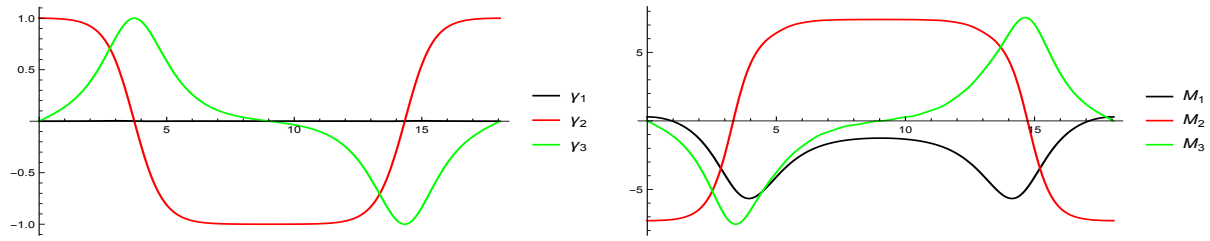

Figure 5. Components γ_j (left) and M_j (right) for the first orbit described in Theorem 3.1.

We note that there exist trivial roll-over orbits as well as trivial heteroclinic orbits. Consider e.g. the manifold $\mathrm{Fix}(S') = \{(\boldsymbol{\gamma}, \boldsymbol{\omega}) \in \mathcal{M} : \gamma_3 = \omega_1 = \omega_2 = 0\}$ that is invariant under the flow. At energy mgb_1, we have a heteroclinic orbit in $\mathrm{Fix}(S')$ between the points $z_\pm = ((\pm 1, 0, 0), \boldsymbol{0})$. For energies below mgb_1, the orbits are all closed and avoid $z_\pm$. For energies above mgb_1, the orbits are closed and clearly roll over $\boldsymbol{e}_2$ with the obvious definition of such a roll-over.

Next, we consider some stationary solutions. A stationary point $x = (\boldsymbol{\gamma}, \boldsymbol{\omega})$ necessarily satisfies $\boldsymbol{\omega} = \pm\|\boldsymbol{\omega}\|\boldsymbol{\gamma}$, since $\dot{\boldsymbol{\gamma}} = \boldsymbol{\gamma} \times \boldsymbol{\omega}$ has to vanish. The stability of x is best discussed in terms of the vector field $X : (\boldsymbol{\gamma}, \boldsymbol{\omega}) \mapsto (\dot{\boldsymbol{\gamma}}, \dot{\boldsymbol{\omega}})$. If x is invariant under R, RS, or RS', then the set of eigenvalues λ of $DX(x)$ is invariant under $\lambda \mapsto \bar{\lambda}$ and $\lambda \mapsto -\lambda$.

The simplest stationary points are $x_j = (\boldsymbol{e}_j, \boldsymbol{0})$, where $\boldsymbol{e}_j$ is the unit vector parallel to the j-th coordinate axis. A straightforward computation shows that, besides two eigenvalues zero (due to the conservation of ℓ and $\mathcal{H}$), $DX(x_1)$ has four real eigenvalues, $DX(x_2)$ has two real and two imaginary eigenvalues, and $DX(x_3)$ has four imaginary eigenvalues. This holds for any ellipsoid body with $b_1 > b_2 > b_3 > 0$.

The stationary point x_3 is part of a family of stationary points $z_c = (\boldsymbol{e}_3, c\,\boldsymbol{e}_3)$ parametrized by a real number c. The stability of these points has been investigated in several

papers, including [7,8,9,11,18]. The consensus is that, for many choices of parameters, an analogue of the following holds.

Lemma 3.2. *Consider the parameter values (1.9). There exists a constant $c_* = 1.048\ldots$ such that the stationary point z_c is repelling for $c < -c_*$, hyperbolic for $0 < |c| < c_*$, and attracting for $c > c_*$, if the flow is restricted to the surface $\mathcal{M}_E$ of constant energy $E = \mathcal{H}(z_c)$.*

A pencil-and-paper proof of this lemma is possible, but tedious; so we carried out the necessary (rigorous) computations with a computer. Notice that it suffices to prove the assertions for $c > 0$, since $DX(z_{-c}) = DX(Rz_c) = -DX(z_c)$ by R-reversibility. We remark that Lemma 3.2 excludes the existence of a real analytic first integral that is independent of ℓ and $\mathcal{H}$. A result on the non-existence of analytic integrals was proved also in [16].

Finally, let us describe two one-parameter families of RS'-invariant stationary points. We have not found them discussed in the literature.

Lemma 3.3. *Consider the parameter values (1.9) and points $z = (\boldsymbol{\gamma}, \boldsymbol{\omega})$ with $\gamma_3 = 0$ and $\boldsymbol{\omega} = \pm\|\omega\|\boldsymbol{\gamma}$. There exist a real number $q_* = 0.025941\ldots$ such that the following holds. If $-q_* < \frac{\gamma_1}{\gamma_2} \le 0$, then z is a stationary point. For $\gamma_1 = 0$ we have $\|\omega\| = 0$, and $\|\omega\| \to \infty$ as $\frac{\gamma_1}{\gamma_2} \to -q_*$ from above. Furthermore, if $0 \le \frac{\gamma_2}{\gamma_1} < q_*$, then z is a stationary point. For $\gamma_2 = 0$ we have $\|\omega\| = 0$, and $\|\omega\| \to \infty$ as $\frac{\gamma_2}{\gamma_1} \to q_*$ from below.*

The existence of stationary points near $(\pm\boldsymbol{e}_2, \mathbf{0})$ or $(\pm\boldsymbol{e}_1, \mathbf{0})$ may be a known fact. What seems surprising is that the two critical solutions (corresponding to $\|\omega\| = \infty$) are related via a rotation by $\frac{\pi}{2}$. This part of Lemma 3.3 is not specific to the choice of parameter values (1.9).

The remaining parts of this paper are devoted to our proofs of the results stated in Sections 2 and 3.

4. Integration and Poincaré sections

The equation (1.1) determines $\dot{\boldsymbol{\omega}}$ as a function of $x = (\boldsymbol{\gamma}, \boldsymbol{\omega})$. Together with the equation $\dot{\boldsymbol{\gamma}} = \boldsymbol{\gamma} \times \boldsymbol{\omega}$, this defined a vector field $X = (\dot{\boldsymbol{\gamma}}, \dot{\boldsymbol{\omega}})$ on $\mathbb{R}^6$. This vector field is considered only in a small open neighborhood of $\mathcal{M}$ in $\mathbb{R}^6$ where it is real analytic. The resulting flow $(t, x) \mapsto \Phi_t(x)$ is then real analytic as well.

In order to construct an orbit for a non-small time-interval $[0, r]$, we partition this interval into m small subintervals $[\tau_{k-1}, \tau_k]$ with $\tau_0 = 0$ and $\tau_m = r$. On successive subinterval, starting with $k = 1$, we solve the initial value problem $\dot{x} = X(x)$ with given initial conditions at time τ_{k-1} via the integral equation

$$x(\tau_{k-1} + t) = x(\tau_{k-1}) + \int_0^t X(x(\tau_{k-1} + s))\, ds\,, \qquad 0 \le t \le \tau_k - \tau_{k-1}\,. \tag{4.1}$$

If $\rho = \tau_k - \tau_{k-1}$ is a sufficiently small positive real number, then for $1 \le j \le 6$, the function g defined by $g(t) = x_j(\tau_{k-1} + t)$ is given by its Taylor series about $t = 0$ and has a finite

norm

$$\|g\| = \sum_{n=0}^{\infty} |b_n| \rho^n \,, \qquad b_n = \frac{g^{(n)}(0)}{n!} \,. \tag{4.2}$$

This norm is convenient for computer-assisted proofs, since it is easy to estimate, and since the corresponding function space $\mathcal{G}_\rho$ is a Banach algebra for the pointwise product of functions. Each function $g \in \mathcal{G}_\rho$ extend analytically to the complex disk $|z| < \rho$ and continuously to its boundary. In what follows, ρ is a fixed but arbitrary positive real number.

Consider now the integral equation (4.1), with $k = 1$ to simplify the discussion. Let $x_0(t) = x(0)$. Since the vector field X defines an analytic function on some open neighborhood of $x(0)$, the equation (4.1) can be solved order by order by iterating the transformation $\mathcal{K}$ given by

$$(\mathcal{K}(x))(t) = x_0 + \int_0^t X(x(s))\, ds \,, \tag{4.3}$$

starting with $x = x_0$. That is, the Taylor polynomial x_n of order n for $\mathcal{K}^n(x_0)$ agrees with the Taylor polynomial of order n for x.

This is of course the well-known Taylor integration method. In order to estimate the higher order correction $x - x_d$ for some large degree d, we use a norm on $\mathcal{G}_\rho^6$ of the form

$$\|x\| = \max_{1 \le j \le 6} w_j \|x_j\| \,, \tag{4.4}$$

with appropriately chosen weights $w_j > 0$. A common approach is to apply the contraction mapping theorem on a ball centered at x_d. Instead, we use Theorem 5.1 in [19], which only requires that some closed higher-order set gets mapped into itself. In our programs, the radius ρ and the weights w_j are chosen adaptively, depending on properties of $X(x_d)$.

Computing $\mathcal{K}(x)$ from the Taylor series for x involves only a few basic operations like sums, products, antiderivatives, multiplicative inverses, and square roots. This is done by decomposing each function g involved into a Taylor polynomial g_d of some (large) degree d and a higher order remainder $g - g_d$. For sums, products, and antiderivatives of functions in $\mathcal{G}_\rho$, it is trivial to estimate the higher order remainder of the result.

Consider now the multiplicative inverse $1 + h$ of a function $1 + g$, where

$$g = g_\infty \,, \quad g_n(t) = \sum_{k=1}^{n} b_k t^k \,, \qquad h = h_\infty \,, \quad h_n(t) = \sum_{k=1}^{n} c_k t^k \,. \tag{4.5}$$

The following is straightforward to prove.

Proposition 4.1. *Let $g \in \mathcal{G}_\rho$ with $\|g\| < 1$. Then $h = (1+g)^{-1} - 1$ belongs to $\mathcal{G}_\rho$. The Taylor coefficients c_n of h are given recursively by*

$$c_n = -b_n - \sum_{k=1}^{n-1} b_k c_{n-k} \,, \qquad n = 1, 2, \ldots \tag{4.6}$$

and

$$\|h - h_n\| \le \frac{1}{1 - \|g\|} \big\| 1 - (1+g)(1+h_n) \big\| . \qquad n = 1, 2, \dots \tag{4.7}$$

We note that the same holds if g takes values in some commutative Banach algebra $\mathcal{X}$ with unit. Then the Taylor coefficients b_n and c_n in (4.5) are vectors in $\mathcal{X}$. This fact is used e.g. when estimating the flow for initial points that depend on parameters.

Next, consider the (principal branch of the) square root of a function $1 + g$.

Proposition 4.2. *Let $g \in \mathcal{G}_\rho$ with $\|g\| < \frac{1}{2}$. Then $h = (1+g)^{1/2} - 1$ belongs to $\mathcal{G}_\rho$. The Taylor coefficients c_n of h are given recursively by*

$$c_n = \frac{1}{2} \Big[b_n - \sum_{k=1}^{n-1} c_k c_{n-k} \Big] , \qquad n = 1, 2, \dots \tag{4.8}$$

Furthermore,

$$\|h - h_n\| \le \frac{8}{5} \big\| (1+g) - (1+h_n)^2 \big\| , \qquad n \ge 2 , \tag{4.9}$$

provided that the norm on the right hand side of this inequality does not exceed $\frac{1}{4}$.

Proof. We will use that

$$h - h_n = \frac{1}{2} (1+h_n)^{-1} \big(\big[(1+g) - (1+h_n)^2 \big] - (h - h_n)^2 \big) . \tag{4.10}$$

Verifying this identity and (4.8) is straightforward.

Let now $n \ge 2$. Using the power series for $z \mapsto (1+z)^{1/2} - 1$, and the fact that $\big| \binom{1/2}{k} \big| \le \frac{1}{8}$ for $k \ge 2$, one easily finds that $\|h_n\| \le \frac{5}{8} \|g\|$. This in turn yields a bound $\big\| (1+h_n)^{-1} \big\| \le \frac{8}{5}$. So from (4.10) we find that $\delta = \frac{4}{5} \|h - h_n\|$ satisfies

$$\delta^2 - \delta + \tfrac{16}{25} \varepsilon \ge 0 , \qquad \varepsilon \stackrel{\text{def}}{=} \big\| (1+g) - (1+h_n)^2 \big\| . \tag{4.11}$$

Assuming that $\varepsilon \le \frac{1}{4}$, this implies the bound (4.9). **QED**

Next, we consider the problem of constructing reversible orbits for the given flow. In what follows, we will use $\boldsymbol{M}$ as a primary variable instead of $\boldsymbol{\omega}$. The equation of motion in the variables $(\boldsymbol{\gamma}, \boldsymbol{M})$ is given by

$$\dot{\boldsymbol{\gamma}} = \boldsymbol{\gamma} \times \boldsymbol{\omega} , \qquad \dot{\boldsymbol{M}} = mg\, \boldsymbol{r} \times \boldsymbol{\gamma} + \boldsymbol{M} \times \boldsymbol{\omega} + m \dot{\boldsymbol{r}} \times (\boldsymbol{\omega} \times \boldsymbol{r}) . \tag{4.12}$$

Here, $\boldsymbol{r}$ and $\dot{\boldsymbol{r}}$ are obtained from (1.3), while $\boldsymbol{\omega}$ is determined from $\boldsymbol{r}$ and $\boldsymbol{M}$ via (2.2). In order to simplify notation, we will now write $x = (\boldsymbol{\gamma}, \boldsymbol{M})$ and $X = (\dot{\boldsymbol{\gamma}}, \dot{\boldsymbol{M}})$. Recall that R and RS' commute with the change of variables $(\boldsymbol{\gamma}, \boldsymbol{\omega}) \mapsto (\boldsymbol{\gamma}, \boldsymbol{M})$.

For the construction of periodic orbits, it is convenient to consider return maps to some codimension 1 surface Σ. The surfaces used in our analysis are

$$\Sigma_j = \{ (\boldsymbol{\gamma}, \boldsymbol{M}) \in \mathbb{R}^6 : M_j = 0 \} , \tag{4.13}$$

for $j = 1$ or $j = 3$. Since we are exploiting reversibility, only half-orbits or quarter-orbits need to be considered. Each partial orbit starts at some symmetric (meaning R-invariant or RS'-invariant) point. The goal is to determine such a point x, as well as a positive time $\tau = \tau(x)$, such that $\Phi_\tau(x)$ is again symmetric. To this end, we first determine a symmetric numerical approximation $\bar{x}$ for x and an approximation $\bar{\tau}$ for τ. After choosing a real number τ' slightly smaller than $\bar{\tau}$, the associated Poincaré map $\mathcal{P}$ is then defined by setting

$$\mathcal{P}(x) = \Phi_{\tau(x)}(x)\,, \qquad \tau(x) = \min\bigl\{t \in \mathbb{R} : t \geq \tau' \text{ and } \Phi_t(x) \in \Sigma\bigr\}\,, \tag{4.14}$$

for all (symmetric) starting points x in some neighborhood of $\bar{x}$.

Consider now the problem of constructing the orbit described in Theorem 2.1. The starting point at time $t = 0$ is R-invariant and thus of the form $x = (\boldsymbol{\gamma}, \mathbf{0})$. Restricting to $\|\boldsymbol{\gamma}\| = 1$, the possible starting points are parametrized by a vector $\gamma = (\gamma_1, \gamma_2)$ in $\mathbb{R}^2$ of length less than 1. For the Poincaré section we choose $\Sigma = \Sigma_1$. Then $\tilde{x} = \mathcal{P}(x)$ is of the form $\tilde{x} = \bigl(\tilde{\boldsymbol{\gamma}}, \tilde{\boldsymbol{M}}\bigr)$ with $\tilde{M}_1 = 0$. Define $P(\gamma) = \bigl(\tilde{M}_2, \tilde{M}_3\bigr)$.

Lemma 4.3. *There exists a vector $\bar{\boldsymbol{\gamma}} \in \mathbb{S}_2$ such that the following holds. Let $\bar{x} = (\bar{\boldsymbol{\gamma}}, \mathbf{0})$ and $\tau' = 113$. Then the Poincare map $\mathcal{P}$ with $\Sigma = \Sigma_1$ is well-defined and real analytic in an open neighborhood $B_g \times B_M$ of $\bar{x}$ in $\mathcal{M}$. When restricted to B_g, the associated mapping P is real analytic, has a nonsingular derivative, and takes the value $(0, 0)$ at some R-invariant point. Furthermore, all orbits with starting points in $B_g \times \{\mathbf{0}\}$ have Poincaré time $\tau(x) = 113.7359\ldots$, energy $E = 39.683\ldots$, and reverse as described in Theorem 2.1.*

Our proof of this lemma is computer-assisted and will be described in Section 6. Notice that, if $\boldsymbol{\gamma} \in B_g$ is a solution of $P(\gamma_1, \gamma_2) = (0, 0)$, and if we set $x = (\boldsymbol{\gamma}, \mathbf{0})$, then the point $\Phi_\tau(x)$ is R-invariant for $\tau = \tau(x)$. Thus, as described earlier, this implies that $\Phi_T(x) = x$ with $T = 2\tau(x)$. So Theorem 2.1 follows from Lemma 4.3.

In order to construct the orbit described in Theorem 2.3, we use a Poincare map $\mathcal{P}$ with $\Sigma = \Sigma_3$. The starting point x is again R-invariant, but the desired point $\tilde{x} = \mathcal{P}(x)$ is RS'-invariant, meaning that $\gamma_3 = M_3 = 0$. So the goal is to find zeros of the function P defined by $P(\gamma) = \tilde{\gamma}_3$.

Lemma 4.4. *There exists a vector $\bar{\boldsymbol{\gamma}} \in \mathbb{S}_2$ such that the following holds. Let $\bar{x} = (\bar{\boldsymbol{\gamma}}, \mathbf{0})$. Then the Poincare map $\mathcal{P}$ with $\Sigma = \Sigma_3$ and $\tau' = 63$ is well-defined and real analytic in an open neighborhood $B_g \times B_M$ of $\bar{x}$ in $\mathcal{M}$. When restricted to B_g, the associated function P is real analytic and takes the value 0 at some RS'-invariant point. Furthermore, all orbits with starting points in $B_g \times \{\mathbf{0}\}$ have Poincaré time $\tau(x) = 63.57172\ldots$, energy $E = 42.0308\ldots$ and reverse/roll-over as described in Theorem 2.3. The same holds for a two-parameter family of RS'-invariant initial points.*

Our proof of this lemma will be described in Section 6. Notice that, if $\boldsymbol{\gamma} \in B_g$ is a solution of $P(\gamma_1, \gamma_2) = 0$, and if we set $x = (\boldsymbol{\gamma}, \mathbf{0})$, then the point $\Phi_\tau(x)$ is RS'-invariant for $\tau = \tau(x)$. Thus, by R-reversibility, the point $x' = \Phi_{-\tau}(x)$ is RS'-invariant as well. As described earlier, this implies that $\Phi_T(x') = x'$ with $T = 4\tau(x)$. So Theorem 2.3 follows from Lemma 4.4.

Remark 2. A lemma analogous to Lemma 4.4 holds for the orbit described in Theorem 3.1, with RS'-invariant starting points x. Choosing again $\Sigma = \Sigma_3$ and $P = \tilde{\gamma}_3$, the equation that needs to be solved is $P(\gamma_1, M_1, M_2) = 0$. Here, the value of τ' used in (4.14) is $\tau' = 8.5$.

5. Stationary points and heteroclinic orbits

Consider the flow on $\mathbb{R}^6$ in the variables $(\boldsymbol{\gamma}, \boldsymbol{\omega})$. Clearly, $\bar{x} = ((0,0,\gamma_3),(0,0,\omega_3))$ is a stationary point for any real values $\gamma_3 \neq 0$ and ω_3. So the derivative $DX(\bar{x})$ has two trivial eigenvalues 1, with eigenvectors $((0,0,u),(0,0,v))$. The remaining eigenvalues agree with those of the 4×4 matrix $PDX(\bar{x})P^\top$, where P is the 4×6 matrix defined by $P(\boldsymbol{\gamma}, \boldsymbol{\omega}) = (\gamma, \omega)$, with $\gamma = (\gamma_1, \gamma_2)$ and $\omega = (\omega_1, \omega_2)$.

In what follows, we fix $\gamma_3 = 1$ in the definition of $\bar{x}$. Define two 2×2 matrices J and B by setting

$$J = d^{-1} \begin{bmatrix} \mathbb{I}_{22} + mb_3^2 & -\mathbb{I}_{12} \\ -\mathbb{I}_{21} & \mathbb{I}_{11} + mb_3^2 \end{bmatrix}, \qquad B_{ij} = J_{i,j} m b_j^2 \,, \tag{5.1}$$

where $d = \big(\mathbb{I}_{11} + mb_3^2\big)\big(\mathbb{I}_{22} + mb_3^2\big) - \mathbb{I}_{12}\mathbb{I}_{21}$. Notice that J is the inverse of $P[\mathbb{I} + K(\bar{\boldsymbol{r}})]P^\top$. A straightforward computation shows that

$$PDX(\bar{x})P^\top = \mathcal{L}(\omega_3) = \mathcal{L}_0 + \omega_3 \mathcal{L}_1 + \omega_3^2 \mathcal{L}_2 \,, \tag{5.2}$$

where

$$\mathcal{L}_0 = \begin{bmatrix} 0 & 0 & -J_{21} & -J_{22} \\ 0 & 0 & J_{11} & J_{12} \\ 0 & mg(b_3 - a_2) & 0 & 0 \\ -mg(b_3 - a_1) & 0 & 0 & 0 \end{bmatrix}, \tag{5.3}$$

$$\mathcal{L}_1 = \begin{bmatrix} -B_{21} & 1 - B_{22} & 0 & 0 \\ -1 + B_{11} & B_{12} & 0 & 0 \\ 0 & 0 & -\mathbb{I}_{33} J_{21} & 1 - \mathbb{I}_{33} J_{22} \\ 0 & 0 & -1 + \mathbb{I}_{33} J_{11} & \mathbb{I}_{33} J_{12} \end{bmatrix}, \tag{5.4}$$

and

$$\mathcal{L}_2 = \begin{bmatrix} 0 & 0 & 0 & 0 \\ 0 & 0 & 0 & 0 \\ -\mathbb{I}_{33} B_{21} & -\mathbb{I}_{33} B_{22} & 0 & 0 \\ \mathbb{I}_{33} B_{11} & \mathbb{I}_{33} B_{12} & 0 & 0 \end{bmatrix}. \tag{5.5}$$

Here $a_1 = b_1^2/b_3$ and $a_2 = b_2^2/b_3$ are the principal radii of curvature of the ellipsoid at $r_1 = r_2 = 0$ and $r_3 = \pm b_3$,

Sketch of a proof of Lemma 3.2. Our aim is to apply the Routh-Hurwitz criterion, which is commonly used for such stability problems. It involves the coefficients $p_0, \dots, p_4$ of the characteristic polynomial

$$\det\big(\mathcal{L}(\omega_3) - \lambda \mathrm{I}\big) = \sum_{n=0}^{4} p_n(\omega_3) \lambda^n \,, \tag{5.6}$$

and two other polynomials p_5 and p_6 that are constructed from the coefficients $p_0, \dots, p_4$. By the Routh-Hurwitz criterion, the eigenvalues $\lambda = \lambda(\omega_3)$ of $\mathcal{L}(\omega_3)$ all have a negative real part if and only if $p_n(\omega_3) > 0$ for all n. For the parameters values (1.9), an explicit computation shows that $\deg(p_n) = 4 - n$ for $n \le 4$ and $\deg(p_n) = n - 2$ for $n > 4$. Furthermore, each polynomial p_n is either even or odd; and up to a factor d^4, its coefficients are rationals with denominators that are powers of 2. The value of c_* mentioned in Lemma 3.2 is the positive zero of p_5. The other polynomials p_n have no zeros on the positive real line, as can be seen immediately from their coefficients. The source code of our program `Hurwitz` that computes all these coefficients can be found in [22]. **QED**

Consider now the two orbits described in Theorem 2.2. The first orbit is chosen to pass at time $t = 0$ through the point $x = (\boldsymbol{\gamma}, \mathbf{0})$ with $\gamma_1 = -43585 \times 2^{-17} = -0.3325\ldots$ and $\gamma_2 = -144635 \times 2^{-20} = -0.1379\ldots$. Since x is R-invariant, the orbit of x is R-symmetric. The energy of x is $E = \mathcal{H}(x) = mbs$, with s given by (1.3). The claim is that $\Phi_t(x)$ approaches one of the above-mentioned stationary points $\bar{x} = (\boldsymbol{e}_3, \omega_3 \boldsymbol{e}_3)$ as $t \to \infty$. The value of $\omega_3 > 0$ is determined by the equation $E = \frac{1}{2}\mathbb{I}_{33}\omega_3^2 + mgb_3$.

The second orbit mentioned in Theorem 2.2 passes at time $t = 0$ through the point $x = (\boldsymbol{e}_3, (M_1, M_2, 0))$ with $M_1 = -285332 \times 2^{-20} = -0.2721\ldots$, and with $M_2 < 0$ determined by prescribing the energy $E = 252819 \times 2^{-12} = 61.72\ldots$. Since x is RS-invariant, the orbit of x is RS-symmetric. Defining $\omega_3 > 0$ by the equation $E = \frac{1}{2}\mathbb{I}_{33}\omega_3^2 + mgb_3$, the claim is that $\Phi_t(x)$ approaches the stationary point $\bar{x} = (\boldsymbol{e}_3, \omega_3 \boldsymbol{e}_3)$ as $t \to \infty$.

In both cases, the goal is to prove that there exists a time $\tau > 0$ such that $\Phi_\tau(x)$ belongs to an open neighborhood of $\bar{x}$ in $\mathcal{M}_E$ that is attracted to $\bar{x}$ under the flow. To this end, consider the map $P_E : \mathcal{M}_E \to \mathbb{R}^4$ given by $P_E(x) = Px$, where P is as defined at the beginning of this section. Then the equation of motion on $\mathcal{M}_E$ near the origin is conjugate via P_E to the equation

$$\dot{y} = Y(y)\,, \qquad y = (\gamma_1, \gamma_2, \omega_1, \omega_2)\,, \tag{5.7}$$

where $Y = PX \circ P_E^{-1}$ in some open neighborhood of $\bar{x}$ in $\mathcal{M}_E$. The stationary point for the associated flow is $\bar{y} = 0$.

Notice that $DY(0) = \mathcal{L}(\omega_3)$. Using Lemma 3.2, we have chosen $\bar{x}$ in such a way that $\omega_3 > c_*$. So we know that all eigenvalues of $\mathcal{L}(\omega_3)$ have a negative real part. We expect that all eigenvalues are simple. Then there exists an inner product $\langle \cdot\,, \cdot \rangle$ on $\mathbb{R}^4$ such that the matrix

$$\Lambda = \frac{1}{2}\big[\mathcal{L}(\omega_3) + \mathcal{L}(\omega_3)^*\big] \tag{5.8}$$

is strictly negative, where $\mathcal{L}(\omega_3)^*$ denotes the adjoint of $\mathcal{L}(\omega_3)$ with respect to the above-mentioned inner product. Assume for now that Λ is strictly negative, meaning that $\langle u, \Lambda u \rangle$ is negative for every nonzero vector $u \in \mathbb{R}^4$. Then the derivative

$$\frac{d}{dt}\langle y, y \rangle = 2\langle y, \Lambda y \rangle + 2\big\langle y, N(y) \big\rangle\,, \qquad N(y) = Y(y) - \mathcal{L}(\omega_3)y\,, \tag{5.9}$$

is negative, if the nonlinear part $N(y)$ is sufficiently small compared to y.

Let now $y_\tau = P\Phi_\tau(x)$. In order to prove that y_τ is attracted to zero by the flow associated with Y, it suffices to show that y_τ belongs to a ball $\mathcal{B} \subset \mathbb{R}^4$ that is centered at the origin, with the property that $|\langle y, N(y)\rangle| < |\langle y, \Lambda y\rangle|$ for all nonzero $y \in \mathcal{B}$. This property is equivalent to

$$\left|\left\langle u, \vartheta^{-1} N(\vartheta u)\right\rangle\right| < |\langle u, \Lambda u\rangle|\,, \qquad u \in \partial\mathcal{B}\,, \quad 0 < \vartheta \le 1\,. \tag{5.10}$$

Lemma 5.1. *Let $y_\tau = P\Phi_\tau(x)$, with $\tau = 100$ and x as described above. (Either the R-invariant or the RS-invariant choice.) Then there exists an inner product $\langle \cdot, \cdot\rangle$ on $\mathbb{R}^4$ such that $\langle u, \Lambda u\rangle$ is negative for every nonzero $u \in \mathbb{R}^4$. Moreover, there exists $\delta > 0$ such that y_τ belongs to the ball $\mathcal{B} = \{y \in \mathbb{R}^4 : |\langle y, y\rangle|^{1/2} < \delta\}$, and such that the condition (5.10) holds. Furthermore, the orbit for x has the energy and reversing property described in Theorem 2.2.*

Our proof of this lemma is computer-assisted and will be described in Section 6. Notice that $\Phi_t(x) \to \bar{x}$ as $t \to \infty$, since the norm of $y(t) = P\Phi_t(x)$ tends to zero by (5.9) and (5.10). Furthermore $S\bar{x} = \bar{x}$. So by reversibility, $\Phi_t(x)$ converges to $R\bar{x} = RS\bar{x}$ as $t \to -\infty$. In other words, we have a heteroclinic orbit connecting $R\bar{x} = RS\bar{x} = (\boldsymbol{e}, -\omega_3\boldsymbol{e})$ to $x = (\boldsymbol{e}, \omega_3\boldsymbol{e})$. So Theorem 2.2 follows from Lemma 5.1.

In the remaining part of this section, we give a proof of Lemma 3.3, based in part on (trivial) estimates that have been carried out with the aid of a computer [22]. These estimates are specific to the choice of parameters (1.9), but analogous estimates should work for many other choices. The remaining arguments only use that $b_1 \neq b_2$ and $\mathbb{I}_{13} = \mathbb{I}_{23} = 0$.

Sketch of a proof of Lemma 3.3. We consider the equation for a stationary solution $(\boldsymbol{\gamma}, \boldsymbol{\omega})$ with the property that $\gamma_3 = \omega_3 = 0$. Then $\omega = (\omega_1, \omega_2)$ must be parallel to $\gamma = (\gamma_1, \gamma_2)$. So $\omega = \pm\|\omega\|\gamma$. Consider also the condition $\dot{\boldsymbol{M}} = \boldsymbol{0}$. From (4.12) we see that the first two components of $\dot{\boldsymbol{M}}$ vanish automatically. And the condition $\dot{M}_3 = 0$ becomes

$$g(r_1\gamma_2 - r_2\gamma_1) + m^{-1}(M_1\omega_2 - M_2\omega_1) = 0\,. \tag{5.11}$$

This condition can be written as an equation for $r = (r_1, r_2)$ by using that $\gamma_j = -sb_j^{-1}r_j$ and $\omega = \pm\|\omega\|\gamma$. To be more specific, we define two functions $\mathcal{P}$ and $\mathcal{Q}$ by the equation

$$\begin{aligned} \mathcal{P}(r) &= -sg\big(b_2^{-2} - b_1^{-2}\big)r_1r_2\,, \\ s^2\mathcal{Q}(r) &= \big(m^{-1}\mathbb{I}_{12} - r_1r_2\big)\big(b_2^{-4}r_2^2 - b_1^{-4}r_1^2\big) \\ &\quad + \big[m^{-1}(\mathbb{I}_{11} - \mathbb{I}_{22}) + r_2^2 - r_1^2\big]b_1^{-2}b_2^{-2}r_1r_2\,. \end{aligned} \tag{5.12}$$

A straightforward computation shows that (5.11) reduces to

$$\mathcal{P}(r) + \|\omega\|^2\mathcal{Q}(r) = 0\,. \tag{5.13}$$

If we stay away from the zeros of $\mathcal{Q}$, then the condition is satisfied for some value of $\|\omega\|$ if and only if $\mathcal{P}(r)$ and $\mathcal{Q}(r)$ have opposite signs.

In addition to (5.13), we also have the ellipse condition $(r_1/b_1)^2 + (r_2/b_2)^2 = 1$. So define $p(\theta) = \mathcal{P}(r)$ and $q(\theta) = \mathcal{Q}(r)$, using $r_1 = b_1\sin(\theta/2)$ and $r_2 = b_2\cos(\theta/2)$. Both p

and q are 2π-periodic functions, since $\mathcal{P}$ and $\mathcal{Q}$ are even functions of r. In the remaining part of this paragraph, we consider just the parameters (1.9). Restricting θ to the interval $[-\pi, \pi]$, the sign of $p(\theta)$ is just the sign of $-\theta$. So it suffices to determine the sign of $q(\theta)$. This is easily done by using interval arithmetic. By estimating q and its derivative q' on subintervals, one finds that q has exactly two zeros. Finally, using a (rigorous) Newton method, the zeros are located at values $\theta_* = -0.242951\ldots$ and $\theta'_* = 3.13056\ldots$. For details we refer to the source code of the program `RSp_Stat` in [22].

Notice that $\frac{\gamma_1}{\gamma_2} = \frac{b_2}{b_1}\tan(\theta/2)$. When computing these ratios numerically, it appears that the the vector γ for the angle $\theta = \theta_*$ is orthogonal to the vector γ' for the angle θ'_*. The following argument confirms this observation.

Consider now $\mathcal{Q}$ as a function of γ, say $\mathcal{Q}(r) = Q(\gamma)$. Let γ be a solution of $Q(\gamma) = 0$. This property of γ is equivalent to $M_2\omega_1 - M_1\omega_2 = 0$, meaning that $M = (M_1, M_2)$ is parallel to ω. Recall that $M = (\mathbb{I} + mK(r))\omega$, where $K(r) = \|r\|^2\mathrm{I} - rr^\top$. So ω is an eigenvector of $\mathbb{I}+mK(r)$. Equivalently, ω is an eigenvector of $m^{-1}\mathbb{I}-rr^\top$. But ω is parallel to γ, so γ is an eigenvector as well. Setting $\rho = B^{-1}r$ with $B = \operatorname{diag}(b_1, b_2)$, we have

$$\big[m^{-1}\mathbb{I} - B\rho\rho^\top B\big]\gamma = \lambda\gamma\,, \tag{5.14}$$

for some real number λ. This property is equivalent to the condition $Q(\gamma) = 0$.

Using that the matrix $[\cdots]$ in the above equation is symmetric, we also have

$$\big[m^{-1}\mathbb{I} - B\rho\rho^\top B\big]\gamma' = \lambda'\gamma'\,, \qquad \gamma' = \begin{bmatrix} -\gamma_2 \\ \gamma_1 \end{bmatrix}, \tag{5.15}$$

for some real number λ'. Notice that $\rho = -\|B\gamma\|^{-1}B\gamma$. Let $\rho' = -\|B\gamma'\|^{-1}B\gamma'$. Then

$$\big[m^{-1}\mathbb{I} - B\rho'\rho'^\top B\big]\gamma' = \mu\gamma' + \nu\gamma\,, \tag{5.16}$$

for some real numbers μ and ν. Subtracting (5.16) from (5.15) yields

$$B\big[\rho'\rho'^\top - \rho\rho^\top\big]\rho' = (\lambda' - \mu)B^{-1}\rho' - c\nu B^{-1}\rho\,, \tag{5.17}$$

where c is a nonzero constant. Notice that $\rho'\rho'^\top\rho' = \rho'$ and $\rho^\top\rho\rho^\top = \rho^\top$. Thus, multiplying both sides of (5.17) from the left by $\rho^\top B^{-1}$ yields $0 = (\lambda' - \mu)\rho^\top B^{-2}\rho' - c\nu\rho^\top B^{-2}\rho$. But $\rho^\top B^{-2}\rho' = 0$ since $\gamma^\top\gamma' = 0$. This implies that $\nu = 0$. So the equation (5.16) holds with $\nu = 0$, and this is equivalent to $Q(\gamma') = 0$. This proves the claim in Lemma 3.3 concerning the limits with $\|\omega\| \to \infty$. **QED**

6. Computer estimates

What remains to be done is to prove Lemmas 4.3, 4.4, and 5.1. (Our proof of the lemma referred to in Remark 2 is analogous to the proof of Lemma 4.4, so we will not discuss it separately here.) The necessary estimates are carried out with the aid of a computer. This part of the proof is written in the programming language Ada [23] and can be found in [22]. The following is a rough guide for the reader who wishes to check the correctness of our programs.

6.1. Enclosures and data types

By an enclosure for (or bound on) an element x in a space $\mathcal{X}$ we mean a set $X \subset \mathcal{X}$ that includes x and is representable as data on a computer. For points in $\mathbb{R}^n$ this could be rectangles that contains x. Working rigorously with such enclosures is known as interval arithmetic. What we need here are enclosures for elements in Banach spaces, such as functions $g(t) = \sum_n b_n t^n$ in the spaces $\mathcal{G}_\rho$ described earlier. In addition, when considering orbits that depend on parameters (such as initial conditions), the coefficients b_n can be functions themselves.

In our programs, enclosures are associated with a data type. Let $\mathcal{X}$ be a commutative real Banach algebra with unit $\mathbf{1}$. Our data of type `Ball` are pairs `B` $= (\texttt{B.C}, \texttt{B.R})$, where `B.C` and `B.R` are representable numbers, with `B.R` ≥ 0. The enclosure associated with a `Ball B` is the ball $\texttt{B}_{\mathcal{X}} = \{x \in \mathcal{X} : \|x - (\texttt{B.C})\mathbf{1}\| \leq \texttt{B.R}\}$. For specific spaces $\mathcal{X}$, other types of enclosures will be described below. In all cases, enclosures are closed convex subsets of $\mathcal{X}$ that admit a canonical finite decomposition

$$S = \sum_n x_n \texttt{B(n)}_{\mathcal{X}}\,, \tag{6.1}$$

where each x_n is a representable element in $\mathcal{X}$, and where each `B(n)` is a `Ball` centered at $\mathbf{0}$ or at $\mathbf{1}$.

Assume that $\mathcal{X}$ carries a type of enclosures named `Scalar`. For vectors in $\mathcal{X}^3$ we use a `Scalar`-type enclosure for each component. The corresponding data type `SVector3` is simply an `array(1..3) of Scalar`. Our type `Point` defines enclosures for points $x = (\boldsymbol{\gamma}, \boldsymbol{M})$ with $\boldsymbol{\gamma}, \boldsymbol{M} \in \mathcal{X}^3$. But a `Point P` is in fact a 7-tuple `P=(P.Alpha, P.Beta, P.Gamma, P.M, P.Energy, P.YawPi, P.RollPi)`, where the first four components are of type `SVector3`. The component `P.Energy` is a `Scalar` that defines an enclosure for the energy of a point, while `P.YawPi` and `P.RollPi` are integers. More specifically, `P.YawPi` $= (\psi - \psi_0)/\pi$ and `P.RollPi` $= (\phi - \phi_0)/\pi$, where ψ is the lifted yaw-angle and ϕ the lifted roll-angle for points x in the enclosure given by `P`. The type `Point` is defined in the Ada package `Rattleback`.

Consider now a function $g : D \to \mathcal{X}$ on a disk $D = \{z \in \mathbb{C} : |z| < \rho\}$ with representable radius $\rho > 0$. Denote by $\mathcal{G}$ the space of all such functions that admit a Taylor series representation $g(z) = \sum_{n=0}^{\infty} b_n z^n$ and have a finite norm $\|g\| = \sum_{n=0}^{\infty} \|b_n\| \rho^n$. Here $b_n \in \mathcal{X}$ for all n. A large class of enclosures for functions in this space is determined by the type `Taylor1`, which is defined in the Ada package `Taylors1`. Since this type has been used several times before, we refer to [21] for a rough description and to [22] for details.

Our integration method uses a much simpler type named `Taylor`. A `Taylor P` is an `array(0..d) of Scalar`, where d is some fixed positive integer. The associated enclosure is the set

$$\texttt{P}_{\mathcal{G}} = \sum_{n=0}^{d-1} \texttt{P(n)}_{\mathcal{X}} Z^n + \texttt{P(d)}_{\mathcal{G}} Z^d\,, \qquad Z(z) = z\,. \tag{6.2}$$

Here, $\texttt{P(d)}_{\mathcal{G}}$ is obtained from $S = \texttt{P(d)}_{\mathcal{X}}$ by replacing each ball $\texttt{B(n)}_{\mathcal{X}}$ in the decomposition (6.1) of S by the corresponding ball $\texttt{B(n)}_{\mathcal{G}}$. The first d terms in (6.2) provide enclosures for the polynomial part g_{d-1} of a vector $g \in \mathcal{G}$, as defined in (4.5), while the last term provides an enclosure for both the coefficient b_d and the remainder $g - g_d$. A precise definition of

the type `Taylor` is given in the package `ObO` (an abbreviation for order-by-order). For analytic curves with values in $\mathcal{X}^3$ we use `Taylor`-type enclosures for each component via a type `TVector3`, which is simply an `array(1..3) of Taylor`.

Enclosures for real analytic curves $t \mapsto x(t)$ on D, are defined by the type `Curve` that is introduced in the package `Rattleback.Flows`. In our programs, a `Curve C` is a quadruple `(C.Alpha,C.Beta,C.Gamma,C.M)` whose four components are of type `TVector3`. These enclosures are used in our bounds on the integral operator $\mathcal{K}$ defined by (4.3).

We note that the types `Point`, `Taylor`, and `Curve` depend on choice of the Banach algebra $\mathcal{X}$ via the type `Scalar`. In the case $\mathcal{X} = \mathbb{R}$, we instantiate the package `Rattleback` and others with `Scalar => Ball`. For our analysis of the characteristic polynomial (5.6), which depends on two parameters ω_3 and λ, we use an instantiation of `Rattleback` with `Scalar => TTay`, where `TTay` defines enclosures for real analytic functions of two variables. (`Hurwitz.TTay` is a Taylor series in λ whose coefficients are Taylor series in ω_3.)

Another Banach algebra $\mathcal{T}$ that is very useful consists of pairs (u, u'), where $u \in \mathcal{X}$ and $u' \in \mathcal{X}^n$. Addition and multiplication by scalars is as in $\mathcal{X}^{n+1}$. The product of (u, u') with (v, v') is defined as $(uv, uv' + u'v)$. If one thinks of u and v as being functions of n parameters, then u' and v' transform like gradients. Enclosures for element in $\mathcal{T}$ use a data type `Tangent` that is defined in the package `Tangents`. They are used e.g. to obtain bounds on the derivative of Poincaré maps (by using `Scalar => Tangent`) without first having to determine a formula for the derivative.

6.2. Bounds and procedures

The next step is to implement bounds on maps between the various spaces. By a bound on a map $f : \mathcal{X} \to \mathcal{Y}$ we mean a function F that assigns to a set $X \subset \mathcal{X}$ of a given type (say `Xtype`) a set $Y \subset \mathcal{Y}$ of a given type (say `Ytype`), in such a way that $y = f(x)$ belongs to Y whenever $x \in X$. In Ada, such a bound F can be implemented by defining an appropriate `procedure F(X: in Xtype; Y: out Ytype)`. In practice, the domain of `F` is restricted: if `X` does not belong to the domain of `F`, the `F` raises an `Exception` which causes the program to abort.

The type `Ball` used here is defined in the package `MPFR.Floats.Balls`, using centers `B.C` of type `MPFloat` and radii `B.R` ≥ 0 of type `LLFloat`. Data of type `MPFloat` are high-precision floating point numbers, and the elementary operations for this type are implemented by using the open source MPFR library [26]. Data of type `LLFloat` are standard extended floating-point numbers [25] of the type commonly handled in hardware. Both types support controlled rounding. Bounds on the basic operations for this type `Ball` are defined and implemented in `MPFR.Floats.Balls`.

The Ada package that defines a certain type also defines (usually) bounds on the basic operations that involve this type. In particular, bounds on the maps $g \mapsto g^{-1}$ and $g \mapsto g^{1/2}$ on $\mathcal{G}$ are implemented by the procedures `Inv` and `Sqrt`, respectively, in the package `Obo` that defines the type `Taylor`. In the spirit of order-by-order computations, these procedures include an argument `Deg` for the order (degree) that needs to be processed. At the top degree, which corresponds to the last term in (6.2), the procedures `Inv` and `Sqrt` determine bounds on the higher order terms, using the estimate given in Proposition 4.1 and Proposition 4.2, respectively.

Bounds involving the type `Point` are defined mostly in `Rattleback`. This includes a procedure `Ham` that implements a bound on the energy function $\mathcal{H}$, and a procedure `VecField` that implements a bound on the vector field $(\boldsymbol{\gamma}, \boldsymbol{M}) \mapsto (\dot{\boldsymbol{\gamma}}, \dot{\boldsymbol{M}})$. Several other procedures deal with the construction of points (initial conditions) with prescribed properties; their role is described by short comments in our programs.

The package `Rattleback.Flows` implements bounds on the time-t maps Φ_t and various Poincaré maps. The first few procedures deal with the order-by-order computation of cross products and other basic operations. They maintain temporary data, so that lower order computations do not have to be repeated. And some of them can run sub-tasks in parallel, using the standard tasking facilities that are part of Ada [23]. The procedure `VecField` combines these computations into a bound on the vector field $x \mapsto \dot{x}$ as maps between enclosures of the type `Curve`.

A bound on the solution of the integral equation $\mathcal{K}(x) = x$ is implemented by the procedure `Integrate`. After the polynomial part x_d of the solution x has been determined, a bound on $x - x_d$ is obtained by first guessing a possible enclosure $S \subset \mathcal{G}^6$ for this function, and then checking that $x_d + S$ is mapped into itself by the operator $\mathcal{K}$. Using Theorem 5.1 in [19], this guarantees that $\mathcal{K}$ has a unique fixed point in $x_d + S$. We note that `Integrate` first determines a proper value of the domain parameter ρ for the space $\mathcal{G} = \mathcal{G}_\rho$. This defines the time-increments $\tau_k - \tau_{k-1}$ used in (4.1).

Poincaré maps are now straightforward to implement. The type `Flt_Affine` specifies an affine functional $F : \mathcal{X}^6 \to \mathcal{X}$ whose zero defines a Poincaré section Σ. To be more specific, $F(\boldsymbol{\gamma}, \boldsymbol{M})$ only depends on $\boldsymbol{M}$. Besides an argument `F` that specifies F, the procedure `Sign_Poincare` also includes an argument `TNeed` for the time τ' that enters the definition (4.14). Now `Sign_Poincare` uses (an instantiation of) the procedure `Generic_Flow` to iterate `Integrate`, until $\Phi_t(x)$ with $t \geq \tau'$ lies on Σ. A bound on the zero of $t \mapsto F(\Phi_t(x))$ is determined by using the Newton-based procedure `ObO.FindZero`. We note that t is of type `Scalar`, so the stopping time $\tau = \tau(x)$ can depend on parameters, if $\mathcal{X} \neq \mathbb{R}$.

The angles ψ_0 and ϕ_0 are computed via their definitions (2.1) and (2.3), respectively. This involves integrating the equations $\dot{\boldsymbol{\alpha}} = \boldsymbol{\alpha} \times \boldsymbol{\omega}$ and $\dot{\boldsymbol{\beta}} = \boldsymbol{\beta} \times \boldsymbol{\omega}$ besides (4.12). The lifts of these angles to $\mathbb{R}$ are obtained by estimating their derivatives

$$\dot{\psi} = \frac{\dot{\alpha}_1 \beta_1 - \alpha_1 \dot{\beta}_1}{\alpha_1^2 + \beta_1^2}\,, \qquad \dot{\phi} = \frac{\dot{\gamma}_2 \gamma_3 - \gamma_2 \dot{\gamma}_3}{\gamma_2^2 + \gamma_3^2}\,, \tag{6.3}$$

along the flow. This is done via the procedures `YawNumPi` and `RollNumPi`, respectively, in the package `Rattleback.Flows`. The values of ψ and ϕ at the Poincaré time $\tau(x)$ and the intermediate times $\tau_0, \tau_1, \ldots, \tau_m$ are shown on the standard output. Our claims concerning reversals and roll-over can be (and have been) verified by inspecting the output of our programs.

6.3. Main programs

Our proof of Lemma 4.3 is organized in the programs `R_Der` and `R_Point`. The initial point $x = (\boldsymbol{\gamma}, \mathbf{0})$ is determined from data of type `Point` that are read from a file [22]. It suffices to control the map P described before Lemma 4.3 on a square centered at $\gamma = (\gamma_1, \gamma_2)$.

The chosen square is $2\varepsilon \times 2\varepsilon$, with $\varepsilon = 2^{-2000}$. This square also determines a domain $B_g \subset \mathbb{S}_2$ via the constraint $\|\boldsymbol{\gamma}\| = 1$.

After instantiating the necessary packages, the program `R_Der` computes an enclosure for the derivative DP on R and saves the result to a file. It also verifies that $B_g \times B_M$ belongs to the domain of the Poincaré map for some open neighborhood B_M of the origin in $\mathbb{R}^3$. The program `R_Point` uses the above-mentioned enclosure for DP to verify that a quasi-Newton map associated with P maps R into its interior.

The necessary bounds for Lemma 4.4 are verified using the program `RSpR_Point`. The program takes an argument `Sign_DG1` with values in $\{-1, 0, 1\}$. The starting point is of the form $x = (\boldsymbol{\gamma}, \mathbf{0})$, with $\gamma_2 = -125174 \times 2^{-17}$. If `Sign_DG1` $= 0$, then the value of γ_1 ranges in the interval $[-\delta, \delta]$, where $\delta = 2^{-2500}$. To be more precise, the `Point`-type enclosure `P0` for x is chosen to include an open subset of $\mathcal{M}$, with `P0.Gamma(1)` including $[-\delta, \delta]$. In this case, `RSpR_Point` merely verifies that `P0` is included in the domain of the associated Poincaré map. If `Sign_DG1` $= \pm 1$, then $\gamma_1 = \pm\delta$. In these cases, `RSpR_Point` computes and shows an interval containing $\tilde{\gamma}_3 = P(\gamma)$. Inspecting the output confirms that the sign of $\tilde{\gamma}_3$ agrees with the sign of `Sign_DG1`. Thus, there exist a value $\gamma_1 \in [-\delta, \delta]$ such that $P(\gamma_1, \gamma_2) = 0$.

An additional program `RSpR_Der` can be used (optionally) to prove that DP is nonzero. This implies that the two-parameter family mentioned in Lemma 4.4 is real analytic.

The bounds referred to in Remark 2 are verified via the program `Roll_Point`. This program is analogous to `RSpR_Point`. And there is an analogue `Roll_Der` of `RSpR_Der`.

The bounds needed for Lemma 5.1 are organized by the programs `Het`, `HetRS`, and `Basin`. Both `Het` and `HetRS` run `Plain_Flow` for a time $\tau = 100$. The initial point x is as described in Section 5. Enclosures for x and $\Phi_\tau(x)$ are saved to data files. These files are then read by the procedure `Check` in `Basin`.

An upper bound `LambdaMax` on the spectrum of the (negative) linear operator Λ defined by (5.8) is determined and shown by `Basin.Show_Linear`. This is done by via approximate diagonalization. The matrix that diagonalizes Λ approximately also defines the inner product used in (5.10). Then `Basin.Show_NonLinear` computes and shows an upper bound on the absolute value of the ratio $\langle y, \vartheta^{-1} N(\vartheta y)\rangle / \langle y, y\rangle$ for $y \in \partial\mathcal{B}$. By construction, this bound is non-decreasing in ϑ, so it suffices to consider $\vartheta = 1$. At the end, (5.10) can be (and has been) checked by inspecting the output from `Basic`.

All of these programs were run successfully on a standard desktop machine, using a public version of the gcc/gnat compiler [24]. Instructions on how to compile and run these programs can be found in the file `README` that is included with the source code in [22].

References

[1] G.T. Walker, *On a Curious Dynamical Property of Celt*, Proceedings of the Cambridge Philosophical Society, **8**, 305–306 (1895).

[2] G.T. Walker, *On a dynamical top*, Quarterly Journal of pure and Applied Mathematics **28** 175–184 (1896).

[3] S.A. Chaplygin, *On motion of heavy rigid body of revolution on horizontal plane*, Proceedings of the Society of Friends of Natural Sciences **9**, 10–16 (1897).

[4] R.L. Devaney, *Reversible diffeomorphisms and flows*, Transactions AMS **218**, 89–113 (1976).
[5] R.L. Devaney, *Blue sky catastrophes in reversible and Hamiltonian systems*, Indiana Univ. Math. **26**, 247–263 (1977).
[6] R.E. Lindberg jr., R.W Longman, *On the dynamic behavior of the wobblestone*, Acta Mech. **49**, 81–94 (1983).
[7] A.P. Markeev, *On the dynamics of a solid on an absolutely rough plane*, J. Appl. Math. Mech. **47**, 473–478 (1983).
[8] H. Bondi, *The rigid body dynamics of unidirectional spin*, Proc. R. Soc. Lond. A **405**, 265–274 (1986).
[9] A. Garcia, M. Hubbard, *Spin reversal of the rattleback: theory and experiment*, Proc. R. Soc. Lond. A **418**, 165–197 (1988).
[10] M. Golubitsky, M. Krupa, C. Lim, *Time-reversibility and particle sedimentation*, SIAM J. Appl. Math. **51**, 49–72 (1991).
[11] M. Pascal, *Asymptotic solution of the equations of motion for a Celtic stone*, PMM U.S.S.R **47**, 269–276 (1994).
[12] J.S.W. Lamb, J.A.G. Roberts, *Time-reversal symmetry in dynamical systems: A survey*, Physica D **112**, 1–39 (1998).
[13] A.V. Borisov, I.S. Mamaev, *Strange attractors in rattleback dynamics*, Physics – Uspekhi **46**, 393–403 (2003).
[14] S.V. Gonchenko, I.I. Ovsyannikov, C. Simó, D. Turaev, *Three-dimensional Hénon-like maps and wild Lorenz-like attractors*, Int. J. Bif. And Chaos **15**, 3493–3508 (2005).
[15] A.V. Borisov, A.A. Kilin, I.S. Mamaev, *New effects in dynamics of rattlebacks*, Doklady Physics **51**, 272–275 (2006).
[16] H.R. Dullin, A.V. Tsygvintsev, *On the analytic non-integrability of the Rattleback problem*, Ann. Faculté sciences Toulouse: Math **6,17**, 495–517 (2008).
17] A.V. Borisov, A.Y. Jalnine, S.P. Kuznetsov, I.R. Sataev, J.V. Sedova, *Dynamical phenomena occurring due to phase volume compression in nonholonomic model of the rattleback*, Regul. Chaot. Dyn. **17**, 512–532 (2012).
[18] L. Franti, *On the rotational dynamics of the rattleback*, Cent. Eur. J. Phys. **11**, 162–172 (2013).
[19] G. Arioli, H. Koch, *Existence and stability of traveling pulse solutions of the FitzHugh-Nagumo equation*, Nonlinear Analysis **113**, 51–70 (2015).
[20] Y. Kondo, H. Nakanishi, *Rattleback dynamics and its reversal time of rotation*, Phys. Rev. E **95**, 062207, 11pp (2017).
[21] G. Arioli, H. Koch, *Spectral stability for the wave equation with periodic forcing*, J. Differ. Equations, **265**, 2470–2501 (2018).
[22] G. Arioli, H. Koch, The source code for our programs, data files, and some videos are available at web.ma.utexas.edu/users/koch/papers/rback/
[23] Ada Reference Manual, ISO/IEC 8652:2012(E), available e.g. at www.ada-auth.org/arm.html
[24] A free-software compiler for the Ada programming language, which is part of the GNU Compiler Collection; see gnu.org/software/gnat/
[25] The Institute of Electrical and Electronics Engineers, *IEEE Standard for Floating-Point Arithmetic*, in IEEE Std 754-2019, 1-84 (2019). doi: 10.1109/IEEESTD.2019.8766229
[26] The MPFR library for multiple-precision floating-point computations with correct rounding; see www.mpfr.org/